JOURNAL OF GUIDANCE, CONTROL, AND DYNAMICS
Vol. 29, No. 4, July–August 2006

Aeroelastic System Identification Using the Minimum Model Error Method

Oleg V. Shiryayev* and Joseph C. Slater†
Wright State University, Dayton, Ohio 45435

The minimum model error method is applied to identify models of a panel undergoing limit-cycle oscillations. This work is focused on identification using free-response position and velocity measurements. The response of the panel was obtained using two discretization approaches: the use of finite differences and Galerkin's method. Data from both transient and steady-state parts of the response are used for identification. The models obtained using the steady-state part of the free response were not able to capture the behavior of the true system. The models obtained using the transient part of the free response were able to capture the behavior of the panel very accurately. Accuracy of identified models of various model orders is also discussed.

Nomenclature

A, $\boldsymbol{Bu}(t)$	=	$n \times n$ linear state matrix, and $n \times 1$ vector of known external excitation
A_l	=	assumed linear model state matrix of the size $n \times n$
a_m, a_s	=	nondimensional modal amplitude
D	=	panel bending stiffness
$\boldsymbol{D}$	=	$l \times 1$ vector containing l samples of vector $\boldsymbol{d}(t)$
$\boldsymbol{d}(t)$	=	$n \times 1$ model error (correction term)
E	=	Young's modulus of the panel
$\boldsymbol{f}[\boldsymbol{x}(t), \dot{\boldsymbol{x}}(t)]$	=	$n \times 1$ vector that includes all system nonlinearities
$f_1, f_2, f_3, \ldots$	=	functions selected using the correlation technique
$\boldsymbol{g}_k$	=	accurate model of the measurement process
H_k	=	derivative of the measurement function
h	=	panel thickness
I	=	3×3 identity matrix
L	=	panel length
M	=	flow Mach number
$\mathcal{M}$	=	$l \times p$ matrix that stores the p tested functions evaluated l times
N_{x0}	=	initial in-plane loading on the panel
n	=	system dimension
$\mathcal{P}$	=	vector of unknown function coefficients
S	=	matrix containing snapshots of system states
t, τ	=	time, nondimensional time
t_0, t_f	=	initial and final times
U	=	fluid velocity
$\boldsymbol{v}_k$	=	zero-mean Gaussian noise of known covariance R_k
$\mathcal{W}$	=	$n \times n$ weighting matrix
w, W	=	vertical deflection of the panel
x	=	coordinate along the panel
$\boldsymbol{x}_l(t)$	=	state vector estimate obtained from the linear model
$\dot{\boldsymbol{x}}(t), \boldsymbol{x}(t)$	=	$n \times 1$ vectors of system states and their derivatives
$\hat{\boldsymbol{x}}(t)$	=	state vector estimated from the corrected linear model
$\tilde{\boldsymbol{y}}(t_k)$	=	$n \times 1$ measurement vector at time t_k
$\alpha, \beta, \gamma, \ldots$	=	unknown function coefficients
Δp	=	static-pressure differential across the panel
$\boldsymbol{\delta}(t)$	=	vector of costates (Lagrange multipliers)
Λ	=	diagonal matrix of eigenvalues
λ	=	nondimensional dynamic pressure
μ	=	nondimensional mass ratio
ξ	=	nondimensional coordinate along the panel
ρ_f	=	fluid mass density
ρ_s	=	plate mass density
Φ	=	transformation matrix
$\phi_m(\xi)$	=	Galerkin trial functions
$0, \boldsymbol{0}$	=	3×3 matrix of zeros, 3×1 vector of zeros

Received 7 December 2004; revision received 5 March 2005; accepted for publication 11 March 2005.

*Graduate Research Assistant, Department of Mechanical and Materials Engineering; shiryayev.2@wright.edu. Student Member AIAA.

†Associate Professor, Department of Mechanical and Materials Engineering; joseph.slater@wright.edu. Associate Fellow AIAA.

Introduction

SYSTEM identification is the process of developing or improving a mathematical model of a given physical system using measurement data from experiments. In general, most mechanical dynamic systems can be divided into two classes, linear systems and nonlinear systems. There are many very well-developed methods for identification of linear systems.[1] Most real-world systems exhibit nonlinearity to some degree. Billings[2] reported that there is a multitude of methods for identification of nonlinear systems. Mook and Junkins[3] have developed the minimum model error (MME) method that allows identification of nonlinear state-space models, and Stry[4] has improved it by adding a correlation technique. The MME method has not been widely applied. However, it is documented that Crassidis and Markley[5] employed the MME approach for attitude estimation.

Intensive research in modeling of aeroelastic systems is concentrated on identification of nonlinear models because such dynamic systems are inherently nonlinear. Various system identification methods have been applied for model estimation from flight-test data. Baldelli et al.[6] used block-oriented identification technique for identification of a pitch-plunge system. Marzocca et al.[7] applied Volterra series approach for modeling a fluttering panel. Volterra kernel theory was also applied for identification of F/A-18 active aeroelastic wing.[8] The primary scope of this paper is to demonstrate the application of the MME system identification algorithm for modeling of a nonlinear aeroelastic system using free-response measurements.

MME Identification Algorithm

The dynamic system identification algorithm consists of two major parts. The first part is the minimum model error estimation technique. Given an assumed linear state-space model and a set of measurements of the states, it estimates the dynamic error trajectories

of the states. The second part employs the correlation technique to select the functions that best correlate to the dynamic error and finds the appropriate coefficients using a least-squares fit.

A general forced nonlinear dynamic system can be represented in state-space form by the following equation:

$$\dot{\boldsymbol{x}}(t) = A\boldsymbol{x}(t) + B\boldsymbol{u}(t) + \boldsymbol{f}[\boldsymbol{x}(t), \dot{\boldsymbol{x}}(t)] \tag{1}$$

Time-domain measurements of the system states are available in the form:

$$\tilde{\boldsymbol{y}}(t_k) = \boldsymbol{g}_k[\boldsymbol{x}(t_k), t_k] + \boldsymbol{v}_k, \qquad t_0 \le t_k \le t_f \tag{2}$$

where $\boldsymbol{v}_k$ represents measurement errors.

To implement MME, an assumed linear model must be chosen. The model could be derived from physics, but it needs not accurately represent the system behavior because the actual system itself is nonlinear or because of difficulty deriving a correct model from the physics. The assumed linear model is given in state-space form as

$$\dot{\boldsymbol{x}}_l(t) = A_l\boldsymbol{x}_l(t) + B\boldsymbol{u}(t) \tag{3}$$

Note that the forcing $B\boldsymbol{u}(t)$ is assumed to be known. MME computes the model error using the assumed model in Eq. (3) and the measurements of the states in Eq. (2). Because the system in Eq. (3) lacks some information, the linear state matrix A_l is not necessarily equal to A from Eq. (1).

The corrected dynamic model is obtained by adding the correction term to the assumed linear model as

$$\dot{\hat{\boldsymbol{x}}}(t) = A_l\hat{\boldsymbol{x}}(t) + B\boldsymbol{u}(t) + \boldsymbol{d}(t) \tag{4}$$

If the model is accurate, then the predicted state vector $\hat{\boldsymbol{x}}(t)$ matches the true state $\boldsymbol{x}(t)$ in Eq. (1) within measurement errors $\boldsymbol{v}_k$. This condition, often referred to as the covariance constraint (see Mook and Junkins[3]), can be written mathematically as

$$\{\tilde{\boldsymbol{y}}(t_k) - \boldsymbol{g}_k[\hat{\boldsymbol{x}}(t_k), t_k]\} \times \{\tilde{\boldsymbol{y}}(t_k) - \boldsymbol{g}_k[\hat{\boldsymbol{x}}(t_k), t_k]\}^T \approx R_k \tag{5}$$

where R_k is the error induced by the measurement equipment, which can be obtained from the specifications supplied by manufacturers, or otherwise it can set by the experimentalist depending on reliability of the measurements.

The optimum model correction $\boldsymbol{d}(t)$ is obtained by minimization of the cost function J:

$$J = \sum_{k=1}^{M} \{\tilde{\boldsymbol{y}}(t_k) - \boldsymbol{g}_k[\hat{\boldsymbol{x}}(t_k), t_k]\}^T \times R_k^{-1} \times \{\tilde{\boldsymbol{y}}(t_k) - \boldsymbol{g}_k[\hat{\boldsymbol{x}}(t_k), t_k]\} + \int_{t_0}^{t_f} \boldsymbol{d}(\tau)^T \mathcal{W}\boldsymbol{d}(\tau)\,\mathrm{d}\tau \tag{6}$$

The weighting matrix $\mathcal{W}$ is obtained such that we find the smallest correction $\boldsymbol{d}(t)$ to make the estimated state trajectories statistically compatible with the measurements. Conditions that are necessary to minimize J are summarized as follows (for details, see Geering[9]):

$$\dot{\hat{\boldsymbol{x}}}(t) = A_l\hat{\boldsymbol{x}}(t) + B\boldsymbol{u}(t) + \boldsymbol{d}(t) \tag{7}$$

$$\dot{\boldsymbol{\delta}}(t) = -A_l^T\boldsymbol{\delta}(t) \tag{8}$$

$$\boldsymbol{d}(t) = -\frac{1}{2}\mathcal{W}^{-1}\boldsymbol{\delta}(t) \tag{9}$$

$$\boldsymbol{\delta}\left(t_k^+\right) = \boldsymbol{\delta}\left(t_k^-\right) + 2H_kR_k^{-1}\{\tilde{\boldsymbol{y}}(t_k) - \boldsymbol{g}_k[\hat{\boldsymbol{x}}(t_k), t_k]\} \tag{10}$$

$$H_k = \left.\frac{\partial \boldsymbol{g}}{\partial \boldsymbol{x}}\right|_{\dot{\boldsymbol{x}}(t_k), t_k} \tag{11}$$

$$\boldsymbol{x}(t_0) = \boldsymbol{x}_0 \qquad \text{or} \qquad \boldsymbol{\delta}(t_0) = 0 \tag{12}$$

$$\boldsymbol{x}(t_f) = \boldsymbol{x}_f \qquad \text{or} \qquad \boldsymbol{\delta}(t_f) = 0 \tag{13}$$

The boundary conditions for the preceding two-point boundary-value-problem (TPBVP) can be such that either $\boldsymbol{x}(t_0)$ and $\boldsymbol{x}(t_f)$ are specified at the initial and final times, or $\boldsymbol{\delta}(t_0) = 0$ and $\boldsymbol{\delta}(t_f) = 0$ are set at the initial and final times. The preceding TPBVP involves jump discontinuities in the costates and thus in the dynamic error term. These jumps decrease the accuracy of the algorithm because it becomes more difficult to identify the appropriate functional form.

Mook and Lew[10] derived a solution to this type of TPBVP by the means of linear algebra. Their solution involves the use of multiple shooting algorithm, which allows one to decrease the negative effect of the jumps. However, multiple shooting restricts the assumed model to be linear. Because Eqs. (7–10) define an optimization problem for a given $\mathcal{W}$, the covariance constraint [see Eq. (5)] must be checked. If this constraint is not satisfied, initial weighting factor $\mathcal{W}$ must be changed, and the entire solution procedure has to be repeated for a new value of $\mathcal{W}$. Otherwise, the model correction term $\boldsymbol{d}(t)$ can be obtained using Eq. (9).

The functional form that is present in the model error estimate can be identified by calculating correlation coefficients between the model error and the functions of the estimated states. The correlation of the actual function is close to, but not exactly equal to, one. The correlation calculated for the functions that are not present in the actual system are close to zero. Once the functional form present in the model is identified, a least-squares fit is used to find the coefficient for this term.

In general, the error term can be expressed as containing more than one functional form as

$$\boldsymbol{d}(t) = \alpha f_1[\boldsymbol{x}(t)] + \beta f_2[\boldsymbol{x}(t)] + \gamma f_3[\boldsymbol{x}(t)] + \cdots \tag{14}$$

In the matrix form the preceding equation can be rewritten as

$$\boldsymbol{D} = \mathcal{M}\mathcal{P} \tag{15}$$

It is suggested to choose the number of samples l to be within center 80% of the number of measurements because it was found that MME converges in that region.[4] The least-squares estimate is found by minimizing the following functional with respect to $\mathcal{P}$:

$$\Gamma = [\boldsymbol{D} - \mathcal{M}\mathcal{P}]^T[\boldsymbol{D} - \mathcal{M}\mathcal{P}] \tag{16}$$

The solution is given by

$$\mathcal{P} = (\mathcal{M}^T\mathcal{M})^{-1}\mathcal{M}^T\boldsymbol{D} \tag{17}$$

This approach allows any kind of function to be used to fit the dynamic error term. In some cases the form of dynamic error term is unknown, and one can find oneself repeatedly guessing for the correct functional form(s) or using a large number of functions. In practice, almost any curve can be accurately represented by summation of a large number of analytical terms. Such a situation decreases the efficiency of the algorithm and yields the models that are too complex for engineering applications. In addition, Mook and Stry[11] showed that if the actual term is not present in the library the correlation technique selects the terms that are in the series expansion of the actual function.

System Geometry and Governing Equations

The two-dimensional panel undergoing limit-cycle oscillations first studied by Dowell[12] is considered here. The plate is pinned at both ends and subject to a supersonic flow over the top surface. The geometry of the problem is shown in Fig. 1. According to Dowell,[12] the governing differential equation for the panel motion employs von Kármán's large deflection theory and is written as

$$D\frac{\partial^4 w}{\partial x^4} - (N_x + N_{x0})\frac{\partial^2 w}{\partial x^2} + \rho_s h\frac{\partial^2 w}{\partial t^2} + (p - p_\infty) = \Delta p \tag{18}$$

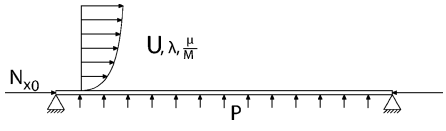

Fig. 1 Panel geometry.

where the in-plane force caused by vertical deflection is represented as

$$N_x = \frac{Eh}{2L}\int_0^L \left(\frac{\partial w}{\partial x}\right)^2 \mathrm{d}x \tag{19}$$

In Eq. (18), $p - p_\infty$ is the aerodynamic pressure loading given by quasi-steady, supersonic theory, also known as piston theory:

$$p - p_\infty = \frac{\rho_f U^2}{\mathcal{B}}\left[\frac{\partial w}{\partial x} + \left(\frac{M^2-2}{M^2-1}\right)\frac{1}{U}\frac{\partial w}{\partial t}\right] \tag{20}$$

In Eq. (20), $\mathcal{B} = \sqrt{(M^2-1)}$, and the aerodynamic load is a function of displacement and velocity along the panel, $p - p_\infty = f[w(x), \dot{w}(x)]$, which results in additional stiffness and damping contribution to the system.

It is possible to rewrite Eq. (18) in the nondimensionalized form as

$$D\frac{\partial^4 W}{\partial \xi^4} - 6(1-\nu^2)\left[\int_0^1 \left(\frac{\partial W}{\partial \xi}\right)^2 \mathrm{d}\xi\right]\frac{\partial^2 W}{\partial \xi^2} - R_x\frac{\partial^2 W}{\partial \xi^2} + \frac{\partial^2 W}{\partial \tau^2} + \lambda\left[\frac{\partial W}{\partial \xi} + \left(\frac{M^2-2}{M^2-1}\right)\left(\frac{\mu}{\beta\lambda}\right)^{\frac{1}{2}}\frac{\partial W}{\partial \tau}\right] = P \tag{21}$$

where the nondimensional parameters are

$$\xi \equiv \frac{x}{L}, \qquad \tau \equiv t\sqrt{\frac{D}{\rho_s h l^4}}, \qquad W \equiv \frac{w}{h}, \qquad \lambda \equiv \frac{\rho_f U^2 l^3}{\beta D}$$

$$\mu \equiv \frac{\rho_f l}{\rho_s h}, \qquad R_x \equiv \frac{N_{x0} l^2}{D}, \qquad P \equiv \frac{\Delta p l^4}{Dh} \tag{22}$$

The nondimensionalized equation of motion can now be put into the state-space form.

Mortara[13] discretized the spatial derivatives of W by using the central, fourth-order finite differences approach. In matrix form this equation becomes

$$\ddot{\boldsymbol{W}} + [C_A]\dot{\boldsymbol{W}} + [K_S - K_N + K_A]\boldsymbol{W} = \boldsymbol{P} \tag{23}$$

where C_A is a damping matrix in which each element represents the aerodynamic damping coefficient for each node of the finite difference model of the panel. The matrices K_A, K_S, and K_N represent the aerodynamic, linear, and nonlinear structural stiffening effects. The nonlinear integral is reevaluated at each time step as

$$\int_0^L (W')^2 \mathrm{d}\xi = \frac{\Delta\xi}{2}\left(\frac{-3W_1 + 4W_2 - W_3}{2\Delta\xi}\right)^2 + \Delta\xi\sum_{i=2}^{i=m-1}\left(\frac{W_{i+1} - W_{i-1}}{2\Delta\xi}\right)^2 + \frac{\Delta\xi}{2}\left(\frac{3W_m - 4W_{m-1} + W_{m-2}}{2\Delta\xi}\right)^2 \tag{24}$$

If the summation of stiffness terms is denoted by $K = K_S - K_N + K_A$, Eq. (23) can be put into the state-space form suitable for numerical integration:

$$\begin{bmatrix}\dot{\boldsymbol{W}}\\ \ddot{\boldsymbol{W}}\end{bmatrix} = \begin{bmatrix}0 & I\\ -K & -C_A\end{bmatrix}\begin{bmatrix}\boldsymbol{W}\\ \dot{\boldsymbol{W}}\end{bmatrix} + \begin{bmatrix}0\\ \boldsymbol{P}\end{bmatrix} \tag{25}$$

Dowell[12] applied Galerkin's method to discretize Eq. (21). When Galerkin's discretization method is used, the solution is presented as a sum of orthogonal trial functions. These trial functions are such that they satisfy the homogeneous boundary conditions. In his work, Dowell[12] chose to represent the solution as a sum of sinusoids:

$$W(\xi,\tau) = \sum_{m=1}^{\infty} a_m(\tau)\phi_m(\xi) = \sum_{m=1}^{\infty} a_m(\tau)\sin(m\pi\xi) \tag{26}$$

Hence, the first mode constitutes a simple half-sine wave, the second mode is represented as a full sine wave, etc. Thus, Eq. (21) can be rewritten as

$$\sum_m a_m(m\pi)^4\sin(m\pi\xi) + \alpha 6(1-\nu^2)\left[\sum_r a_r^2\frac{(r\pi)^2}{2}\right] \times \sum_m a_m(m\pi)^2\sin(m\pi\xi) + R_x\sum_m a_m(m\pi)^2\sin(m\pi\xi) + \sum_m \frac{\mathrm{d}^2 a_m}{\mathrm{d}\tau^2}\sin(m\pi\xi) + \lambda\left[\sum_m a_m(m\pi)\cos(m\pi\xi) + \left(\frac{\mu}{M\lambda}\right)^{\frac{1}{2}}\sum_m \frac{\mathrm{d}a_m}{\mathrm{d}\tau}\sin(m\pi\xi)\right] = P \tag{27}$$

The weighted residual is minimized over the spatial domain according to

$$\int_{\xi=0}^{\xi=1} \Omega(\xi,\tau)\phi_m(\xi)\,\mathrm{d}\xi = 0 \tag{28}$$

where $\Omega(\xi,\tau)$ is the residual and the weighting functions are chosen to be the same as trial functions $\phi_m(\xi)$. Thus, a set of coupled nonlinear differential equations in time is obtained for each of the considered modes:

$$a_s\frac{(s\pi)^4}{2} + \alpha 6(1-\nu^2)\left[\sum_r a_r^2\frac{(r\pi)^2}{2}\right]a_s\frac{(s\pi)^2}{2} + R_x a_s\frac{(s\pi)^2}{2} + \frac{1}{2}\frac{\mathrm{d}^2 a_s}{\mathrm{d}\tau^2} + \lambda\left\{\sum_{m,m\neq s}\frac{sm}{s^2-m^2}[1-(-1)^{s+m}]a_m + \frac{1}{2}\left(\frac{\mu}{M\lambda}\right)^{\frac{1}{2}}\frac{\mathrm{d}a_s}{\mathrm{d}\tau}\right\} = \int_{\xi=0}^{\xi=1} P_1\sin(s\pi\xi)\,\mathrm{d}\xi \tag{29}$$

Dowell[12] concluded that numerical solution converges when six modes are used in approximation. For this study, state-space equations were obtained using six modes.

Data Reduction

Most practical real-world systems fall into the class of distributed parameter systems, but experimental measurements are only available for the locations where sensors are situated. In this work, simulated measurement data are projected onto orthogonal basis functions, which enables model identification of spatially distributed systems.

When the Galerkin method is used for discretization, the state-space equations are written in terms of modal amplitudes so that no data transformation is needed. In the case of the finite difference discretization approach, the measurement data from each individual node do not contain enough information about the behavior of the panel as a whole. Thus, in order to create a reduced-order model, data from all nodes have to be transformed into a form that is suitable for building such model. This can be achieved by projecting the nodal measurement data on the set of operational deflection shapes, otherwise known as basis functions, which are obtained using proper orthogonal decomposition (POD). Holmes et al.[14] have given an extensive overview of the POD method. Epurenau and Dowell[15] have utilized POD in their work for developing reduced-order aeroelastic models.

The idea of POD is to capture the dominant modes of the system by using the snapshots of system states taken in time. Let S be an $n \times m$ matrix where each column is a snapshot of system states taken at a certain time. Consider, the transformation between the full states $\boldsymbol{z}(t)$ and the reduced states $\boldsymbol{x}(t)$ to be written as

$$\boldsymbol{z}(t) = \Phi \boldsymbol{x}(t) \tag{30}$$

Now consider the transformation matrix Φ written as

$$\Phi = SV \tag{31}$$

where V is a set of reduced-order vectors that satisfies the following eigenequation:

$$S^T SV = V\Lambda \tag{32}$$

The magnitude of the eigenvalues in Λ relates to the significance of their respective modes relative to each other. The matrix Φ is then divided into the retained portion Φ_R and the truncated portion Φ_T.

$$\Phi = [\Phi_R \quad \Phi_T] \tag{33}$$

Utilizing the retained modes from matrix Φ, one can compute the reduced states as

$$\boldsymbol{x}(t) = \left(\Phi_R^T \Phi_R\right)^{-1} \Phi_R^T \boldsymbol{z}(t) \tag{34}$$

Experiments

All numerical experiments were performed using double-precision arithmetic in MATLAB.[16] The simulation of panel flutter was performed for the flow speed of Mach 3.7, using the following values of nondimensional parameters:

$$\lambda = 448.17, \qquad h/L = 0.004, \qquad \mu = 0.04$$
$$R_x = 0, \qquad P = 0 \tag{35}$$

Also, the Young's modulus of material of the panel was chosen to be $E = 210$ GPa and Poisson's ratio $\nu = 0.3$. Note that the linear flutter onset point for this configuration is at $\lambda = 343$ (see Dowell[12]) and no external pressure differential was applied [$P = 0$, Eq. (35)]. For the finite difference case, the panel was discretized using 64 nodes. State-space equations were numerically integrated to obtain the time history of panel motion for $\tau \in [0, 6]$, with the time step of 0.0005. Then the obtained data were decimated using a decimation step of three, so that the time resolution of the data supplied to MME was 0.0015. The initial position for the first modal amplitude was set to be equal to 0.2; all of the rest of modal position and velocity amplitudes were set to be zero. This is equivalent to the initial displacement of the panel in the form of half-sine wave with the highest point being set at 0.2 and zero initial velocity.

Simulation was performed using state-space equations obtained from both discretization approaches. The initial part of the response contains the transients. After $\tau \approx 5$, vibration of the panel settles into sustained limit-cycle oscillations. First, 667 data points are taken from the interval $\tau \in [0, 1]$ of the total time history obtained; these data contain the response where transients are present. Then, 667 data points are taken in the interval $\tau \in [5, 6]$; these data contain steady-state oscillations. Two data sets were obtained from state-space model obtained using Galerkin's method, and two data sets were acquired using the model obtained through finite differences. Thus, a total of four data sets were used as an input to MME identification algorithm.

Results

The accuracy of identified models depends on the number of modes that they contain. Ideally, the model should contain the number of modes that dominate the response of the true system. From the analysis of linearized state-space models, it was found that the first two modes are very closely spaced and that they are responsible for the instability of the system. Gopinathan[17] identified a single-degree-of-freedom model to represent limit-cycle oscillations (LCO) of the panel. In this work, in order to include transient capability in the model, three degrees of freedom (DOF) were considered for identification at first.

Identification was performed in two steps. During the first step, the assumed linear system [see Eq. (3)] contains no information about system stiffness and damping as shown in Eq. (36). In her work, Stry[4] states that, to improve accuracy, the assumed initial model should contain as much information about the system as possible. Hence, in the second step the linear part of the model identified after the first step was used as the assumed linear model for the identification algorithm:

$$\begin{bmatrix} \dot{x}_1 \\ \dot{x}_2 \\ \dot{x}_3 \\ \ddot{x}_1 \\ \ddot{x}_2 \\ \ddot{x}_3 \end{bmatrix} = \left[\begin{array}{ccc|ccc} 0 & 0 & 0 & 1 & 0 & 0 \\ 0 & 0 & 0 & 0 & 1 & 0 \\ 0 & 0 & 0 & 0 & 0 & 1 \\ \hline 0 & 0 & 0 & 0 & 0 & 0 \\ 0 & 0 & 0 & 0 & 0 & 0 \\ 0 & 0 & 0 & 0 & 0 & 0 \end{array}\right] \begin{bmatrix} x_1 \\ x_2 \\ x_3 \\ \dot{x}_1 \\ \dot{x}_2 \\ \dot{x}_3 \end{bmatrix} + \begin{bmatrix} d_1 \\ d_2 \\ d_3 \\ d_4 \\ d_5 \\ d_6 \end{bmatrix} \tag{36}$$

The governing equation (21) suggests that the only nonlinear terms present in the system model are the cubic stiffness terms. From Eq. (1), all nonlinearities in the system are represented by the vector $\boldsymbol{f}(\boldsymbol{x}, \dot{\boldsymbol{x}})$. From Galerkin's discretization approach it was found that nonlinear stiffness for the jth degree of freedom is of the following form:

$$f_j = \sum_{i=1}^{3} a_{ij} x_j x_i^2, \qquad j = 1 \ldots 3 \tag{37}$$

where a_{ij} is the coefficient of the corresponding term, x_j is the position of the jth degree of freedom, and x_i is the position of the ith degree of freedom. Thus, for data obtained using Galerkin's method, the only nonlinear terms in the function library were of the form as shown in Eq. (37).

Finite difference discretization does not provide any insight on the form of nonlinear stiffness terms other than that they are cubic. Preliminary identification runs with the same terms as were used for the data from Galerkin's approach [see Eq. (37)] showed that these three terms are not enough to obtain an accurate model for the data obtained using POD. It was found that six terms as written in Eq. (38) are able to provide an accurate model identification.

$$f_j = \sum_{i=1}^{3} a_{j1i} x_1 x_i^2 + \sum_{i=1}^{3} a_{j2i} x_2 x_i^2, \qquad j = 1 \ldots 3 \tag{38}$$

Note that this formulation of Eq. (38) does not contain terms such as

$$\sum_{i=1}^{3} a_{j3i} x_3 x_i^2$$

If these terms had been considered, then all possible cubic combinations would have been included in the model. In fact, almost any data can be fit if a sufficient number of functions is used in approximation. Having too many functions in the model is not desirable because it makes the model too complicated and reduces its engineering applicability.

Identification Using the Transient Data

The models identified after the first step for input data from Galerkin's and the finite differences approaches are presented in Eqs. (39) and (40) respectively. The eigenvalues of the linear parts of the corresponding models are presented in Tables 1 and 2. Note that the true systems defined in Tables 1 and 2 are slightly different because one was obtained from Galerkin's discretization approach [Eq. (29)] and the other from finite differences approach [Eq. (25)]. The real parts of the eigenvalues of the first two modes are within 10% of the true system values.

Further evaluation of identified models was performed by examining their prediction of the panel response. It was not expected that the three-DOF models would match the transient behavior of the panel very closely, and so it was chosen to compare the steady-state

Table 1 Eigenvalues of the true system and identified models (transient data from Galerkin's approach)

Mode number	1	2	3
True system	$7.62 \pm 35.86j$	$-9.83 \pm 35.86j$	$-1.10 \pm 87.83j$
Identified model, step 1	$6.96 \pm 35.92j$	$-10.51 \pm 35.79j$	$-4.63 \pm 86.90j$
Identified model, step 2	$7.14 \pm 35.67j$	$-10.27 \pm 36.16j$	$-4.55 \pm 87.07j$

Table 2 Eigenvalues of the true system and identified models (transient data from POD)

Mode number	1	2	3
True system	$7.12 \pm 36.14j$	$-9.33 \pm 36.14j$	$-1.10 \pm 88.77j$
Identified model, step 1	$6.49 \pm 36.17j$	$-10.08 \pm 36.04j$	$-4.84 \pm 92.34j$
Identified model, step 2	$6.44 \pm 35.98j$	$-9.54 \pm 36.55j$	$-5.13 \pm 91.88j$

amplitude of the response. The predicted displacement of the panel at $\xi = 3/4$ is presented in Figs. 2 and 3. From these figures it can be observed that the nondimensional amplitude of the limit cycle of the true system is approximately 0.62. The amplitude of LCO produced by the model identified after the first step is found to be much closer to that of the true system, whereas the second model overpredicts it.

$$\begin{bmatrix} \dot{\boldsymbol{x}} \\ \ddot{\boldsymbol{x}} \end{bmatrix} = \left[\begin{array}{ccc|ccc} 0 & & & I & & \\ -100.48 & 1201.2 & -52.48 & -2.297 & 0.7808 & -1.0303 \\ -1204.8 & -1571.4 & 2185.7 & -1.028 & -3.1952 & 5.143 \\ -51.597 & 2152.8 & -8327.2 & 0.0315 & -1.8393 & -10.874 \end{array}\right] \times \begin{bmatrix} \boldsymbol{x} \\ \dot{\boldsymbol{x}} \end{bmatrix} + \begin{bmatrix} 0 \\ -347.66x_1^3 \\ -1325.8x_2x_1^2 \\ -3017.3x_3x_1^2 \end{bmatrix} + \begin{bmatrix} 0 \\ -927.91x_1x_2^2 \\ -4102.6x_2^3 \\ -7874.8x_3x_2^2 \end{bmatrix} + \begin{bmatrix} 0 \\ -2811.7x_1x_3^2 \\ -7513.3x_2x_3^2 \\ -29557x_3^3 \end{bmatrix} \tag{39}$$

$$\begin{bmatrix} \dot{\boldsymbol{x}} \\ \ddot{\boldsymbol{x}} \end{bmatrix} = \left[\begin{array}{ccc|ccc} 0 & & & I & & \\ -1014 & 2350 & 2357 & -3.27 & 2.61 & 4.82 \\ -218.60 & -1417 & -3702 & 0.05 & -3.94 & -4.87 \\ -105.50 & 14.47 & -8594 & -0.02 & -0.19 & -9.64 \end{array}\right] \times \begin{bmatrix} \boldsymbol{x} \\ \dot{\boldsymbol{x}} \end{bmatrix} + \begin{bmatrix} 0 \\ -53.19x_1^3 \\ -36.44x_1^3 \\ 14.1x_1^3 \end{bmatrix} + \begin{bmatrix} 0 \\ -63.32x_1x_2^2 \\ 83.83x_1x_2^2 \\ 30.94x_1x_2^2 \end{bmatrix} + \begin{bmatrix} 0 \\ 408.2x_1x_3^2 \\ 243.8x_2x_2^2 \\ -1410x_1x_3^2 \end{bmatrix} + \begin{bmatrix} 0 \\ 93.78x_2x_1^2 \\ -103.1x_2x_1^2 \\ -36.18x_2x_1^2 \end{bmatrix} + \begin{bmatrix} 0 \\ 42.66x_2^3 \\ -78.8x_2^3 \\ 15.41x_2^3 \end{bmatrix} + \begin{bmatrix} 0 \\ -1492x_2x_3^2 \\ 2207x_2x_3^2 \\ 7012x_2x_3^2 \end{bmatrix} \tag{40}$$

Identification Using the Steady-State Data

In this subsection, identification performed on the data taken from the time interval where $\tau \in [5, 6]$ is presented. The models identified in the first step are presented in Eqs. (41) and (42). The eigenvalues of the linear part of the state-space matrix of the true system and those of identified three-DOF models are presented in Tables 3 and 4. In the case with data from Galerkin's discretization approach, there is a large difference between the imaginary parts of the identified models and the true system for the first two modes. Also, the real part of the third mode for the second identified model is positive, indicating an instability that is not the case for the true system. For the case with input data from the finite differences' discretization approach, the real parts of the eigenvalues of the identified models are very different from those of the true system. Comparing the

Table 3 Eigenvalues of the true system and identified models (steady-state data from Galerkin's approach)

Mode number	1	2	3
True system	$7.62 \pm 35.86j$	$-9.83 \pm 35.86j$	$-1.10 \pm 87.83j$
Identified model, step 1	$9.69 \pm 7.96j$	$-11.32 \pm 7.66j$	$-0.408 \pm 36.47j$
Identified model, step 2	$9.66 \pm 8.00j$	$-11.40 \pm 7.65j$	$0.327 \pm 36.49j$

Table 4 Eigenvalues of the true system and identified models (steady-state data from POD)

Mode number	1	2	3
True system	$7.12 \pm 36.14j$	$-9.33 \pm 36.14j$	$-1.10 \pm 88.77j$
Identified model, step 1	$-0.38 \pm 36.78j$	$-0.53 \pm 38.92j$	$-11.24 \pm 111.14j$
Identified model, step 2	$-0.40 \pm 37.88j$	$-0.61 \pm 45.30j$	$-12.15 \pm 110.37j$

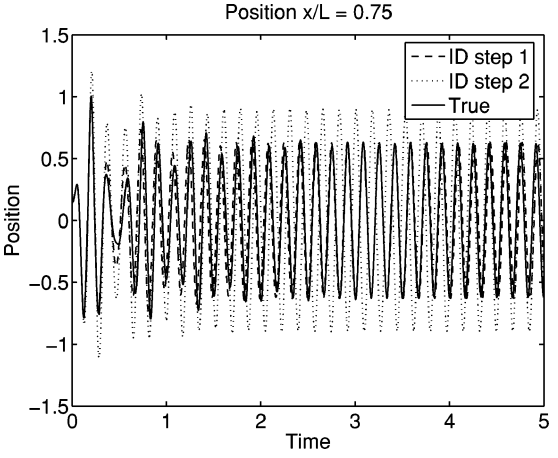

Fig. 2 Position data from Galerkin's approach.

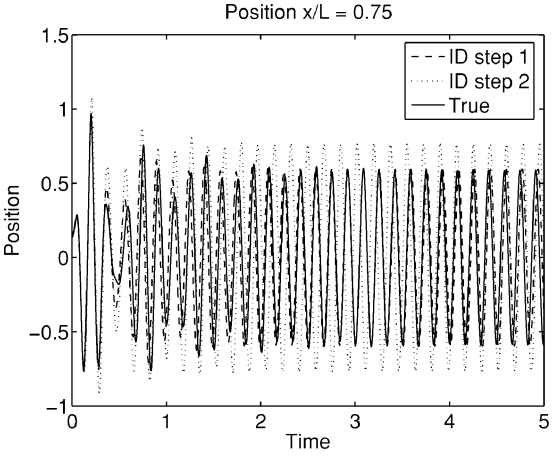

Fig. 3 Position data from finite differences approach.

imaginary parts of the eigenvalues to the case with transient input data, there is a larger discrepancy in the imaginary parts too. Hence, one can conclude that the models identified with the steady-state data from both discretization approaches are not accurate.

The plots of predicted position data obtained from the identified models and that of the true system are presented in Figs. 4 and 5. One can observe that the amplitude and the frequency of the LCO predicted by the models are completely different from those of the true system. In the case with data from the finite differences approach, although the eigenvalues of identified models suggest that they are stable, there are nonlinear terms with positive signs, which make them unstable. MATLAB® was not able to integrate the models from the same initial conditions as the true system. The initial conditions for the data in Fig. 5 were set such that it was possible to integrate the model. Hence, it can be said that the three-DOF models obtained using the steady-state data from both discretization approaches are not valid.

$$\begin{bmatrix}\dot{\boldsymbol{x}}\\ \ddot{\boldsymbol{x}}\end{bmatrix} = \left[\begin{array}{ccc|ccc} 0 & & & I & & \\ \hline -1298 & -41.31 & 0 & -0.77 & 0 & -1.11 \\ -355.59 & 63.11 & 5450.90 & -0.46 & 0.01 & 9.27 \\ 174.07 & 0 & 0 & 0.95 & 0 & -3.30 \end{array}\right] \times \begin{bmatrix}\boldsymbol{x}\\ \dot{\boldsymbol{x}}\end{bmatrix} + \begin{bmatrix} 0 \\ \hline -1494.5x_1^3 \\ 0x_2x_1^2 \\ -8260.4x_3x_1^2 \end{bmatrix} + \begin{bmatrix} 0 \\ \hline -3170.7x_1x_2^2 \\ -189.14x_2^3 \\ -2358.3x_3x_2^2 \end{bmatrix} + \begin{bmatrix} 0 \\ \hline -25219x_1x_3^2 \\ 0x_2x_3^2 \\ -1170.3x_3^3 \end{bmatrix} \tag{41}$$

$$\begin{bmatrix}\dot{\boldsymbol{x}}\\ \ddot{\boldsymbol{x}}\end{bmatrix} = \left[\begin{array}{ccc|ccc} 0 & & & I & & \\ \hline -1426 & 48.01 & 21400 & -0.94 & 5.16 & 35.04 \\ -9.02 & -2022 & -13900 & 0.03 & -0.883 & -20.15 \\ -1.34 & -438.9 & -11910 & 0.08 & -0.15 & -22.48 \end{array}\right] \times \begin{bmatrix}\boldsymbol{x}\\ \dot{\boldsymbol{x}}\end{bmatrix} + \begin{bmatrix} 0 \\ \hline -0.11x_1^3 \\ 1.99x_1^3 \\ 0.18x_1^3 \end{bmatrix} + \begin{bmatrix} 0 \\ \hline -15.85x_1x_2^2 \\ -223.8x_1x_2^2 \\ 227.7x_1x_2^2 \end{bmatrix} + \begin{bmatrix} 0 \\ \hline -2840x_1x_3^2 \\ 1635x_1x_3^2 \\ 1873x_1x_3^2 \end{bmatrix} + \begin{bmatrix} 0 \\ \hline 324.8x_2x_1^2 \\ -103.1x_2x_1^2 \\ -135.2x_2x_1^2 \end{bmatrix} + \begin{bmatrix} 0 \\ \hline 29160x_2^3 \\ 30880x_2^3 \\ -27930x_2^3 \end{bmatrix} + \begin{bmatrix} 0 \\ \hline -91280x_2x_3^2 \\ -173600x_2x_3^2 \\ -160600x_2x_3^2 \end{bmatrix} \tag{42}$$

Effect of Noise on Identification

The effect of noisy measurements on identification accuracy was studied for three-DOF models using measurement data from both discretization approaches. Only the case with data that contains transients was considered. Noisy measurements were obtained by adding 5% noise to the modal data to be supplied to MME. Figures 6 and 7 illustrate noisy displacement measurements for modal data from both discretization approaches.

The models identified from noisy data after the first step were able to reproduce the behavior of the system relatively accurately, although not as accurate as for the case with no noise in the measurement data. The plots of displacement prediction for models identified after the first step using noisy data are shown in Figs. 8 and 9. The models identified from noisy data after the second step were over-

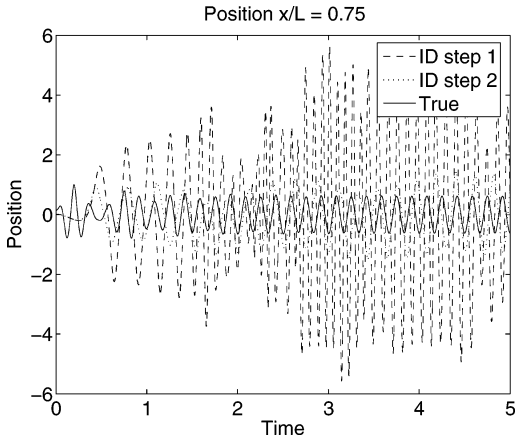

Fig. 4 LCO prediction by models from Galerkin's approach steady-state data.

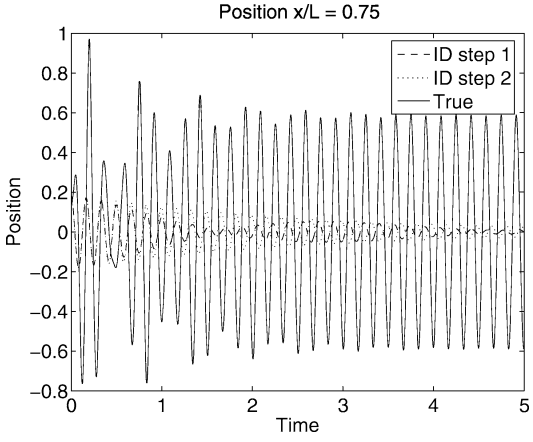

Fig. 5 LCO prediction by models from finite differences approach steady-state data.

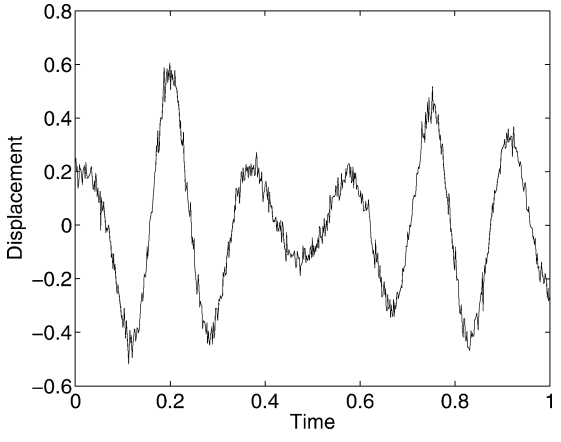

Fig. 6 Noisy displacement measurement for DOF 1, Galerkin's approach.

predicting the LCO amplitude to a much larger degree than those from data without noise. From running several cases with different realizations of noise added to the measurements, it was found that in some cases the models identified after the second step were unstable, indicating that the current implementation of the algorithm failed to yield an accurate model. This implementation allowed the covariance constraint to be satisfied for one of the states as explained later in the paper.

Identification of Four-, Five-, and Six-DOF Models

Because the MME identification technique does not have a theoretical limitation on the order and the size of nonlinear state-space

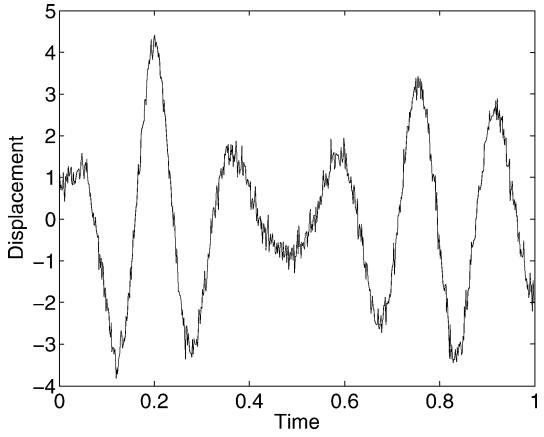

Fig. 7 Noisy displacement measurement for DOF 1, finite differences approach.

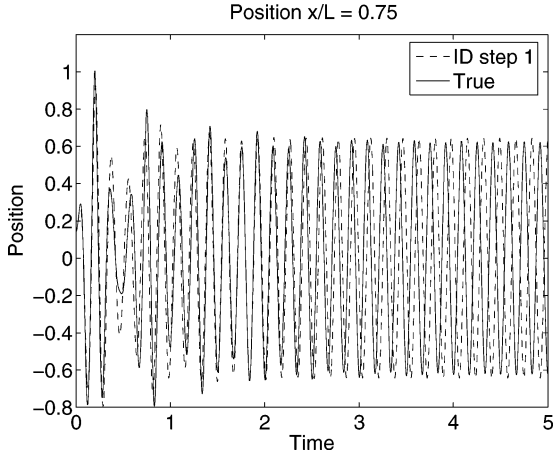

Fig. 8 LCO prediction by model from noisy measurements from Galerkin's approach.

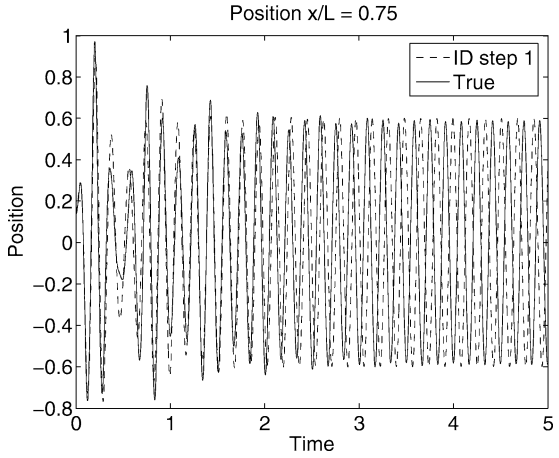

Fig. 9 LCO prediction by model from noisy measurements from finite differences approach.

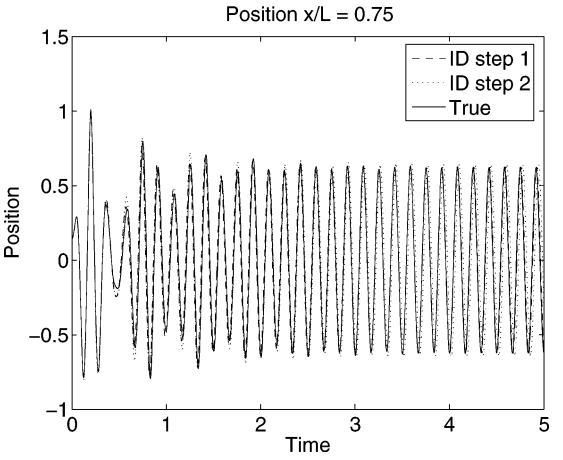

Fig. 10 Six-DOF model LCO prediction.

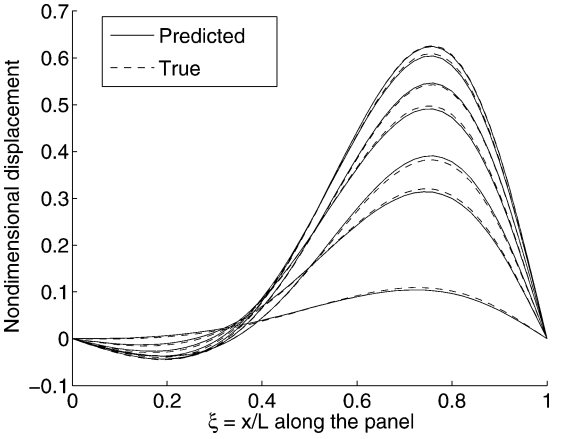

Fig. 11 Snapshots starting at $t = 3.55$ s.

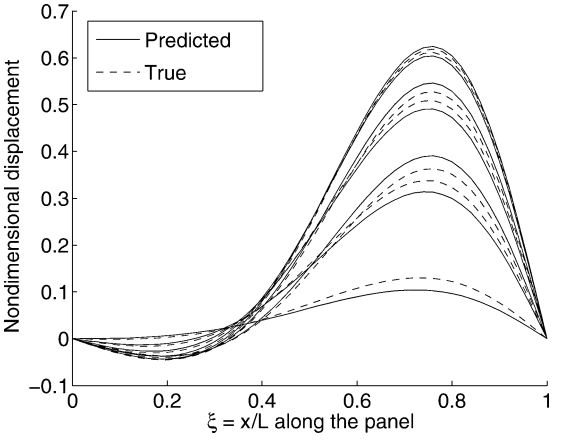

Fig. 12 Snapshots starting at $t = 4.05$ s.

model that can be identified, identification of models of larger sizes was performed. This study was performed using only the data from Galerkin's discretization approach. It was shown that in the case of three-DOF models accurate identification was only possible if data that contained transients were used. Therefore, identification of models of larger sizes was only performed with the transient data.

When MME was applied to the data that contained the transients, all identified models were able to reproduce the behavior of the actual system relatively accurately. For the system considered in this work, it was found that models became more accurate with the increase of the number of DOF. This is expected because the actual model that was used to generate the measurement data contained six DOF. From Fig. 10, one can observe that although the predicted behavior is very close to that of the true system, there is a very small difference in the frequency of oscillations. This implies that the spatial accuracy of the model is time varying. To illustrate this, several consecutive snapshots of the panel taken with an interval of $\Delta\tau = 0.01$ are shown in Figs. 11 and 12. Snapshots in Fig. 11 are taken starting at $\tau = 3.55$, whereas in Fig. 12 the shapshots were taken starting at $\tau = 4.05$. Clearly, the accuracy of spatial prediction of the panel behavior by the identified model is not stationary.

Identification of models that contain more than six DOF was not considered because the additional DOF have no physical

counterparts. The prediction of the panel behavior by the six-DOF models is compared to the true system measurements in Fig. 10. Again, in all cases for four-, five-, and six-DOF models, the additional identification step resulted in the models that were overpredicting the amplitude of LCO.

We believe that the primary reason for the models at the second step to be less accurate than that from the first step is because of the implementation of selection of weighting matrix $\mathcal{W}$ to satisfy the covariance constraint. In theory, $\mathcal{W}$ should be diagonal, and its elements should be different from one another so that the covariance constraint is satisfied for all of the states. It was found from practice that obtaining such $\mathcal{W}$ is a very challenging task. It takes a very long time for optimization routine to obtain the appropriate $\mathcal{W}$, even for simple single-degree-of-freedom nonlinear systems. Hence, a simplified approach was implemented. Current implementation of the algorithm allows the covariance constraint to be satisfied only for the state whose estimate has the largest variation from its measurement. The matrix $\mathcal{W}$ is defined as $\mathcal{W} = \mathcal{C} \cdot I$, where $\mathcal{C}$ is a positive constant. It was found that this provides relatively accurate models when used with an initial model that does not contain any information about the system such as in Eq. (36). This was found to occur with and without noise in the measurement data. (Certainly with noisy measurements identified model accuracy was lower.) However, if applied with the initial linear model that had some information in it, the resulting model appeared to be significantly less accurate. The deficiency of such a simplistic implementation is especially evident from the cases run with noisy measurements, where finding optimum estimates for all states is crucial. The difficulty in obtaining an appropriate weighting matrix is a clear drawback of the MME algorithm.

Conclusions

Two different discretization approaches were used to derive the state-space equations for panel flutter simulation. The data obtained from both simulations were projected on the corresponding basis functions and used as an input to the identification algorithm. For each of the two simulation approaches, input data from two different parts of time history were considered. The results presented in this work show that the models identified from the transient part of the free response were able to reproduce limit-cycle oscillations with reasonable accuracy. The models that were obtained from the steady-state free-response data were not able to reproduce the panel behavior. Thus, it can be concluded that the steady-state free-response data do not contain enough information about the system to identify models that contain several degrees of freedom. Further, the response data that are to be input into the identification algorithm need to be rich enough to contain the necessary information about all degrees of freedom that need to be identified. A potential problem can arise in the case when even the transients in the free response do not contain sufficient information about the system. In such a case forced-response data should be used. Research is to be done to apply the minimum model error identification technique to modeling of a fluttering panel using forced-response measurements.

In this work, the state-space models were identified for a single realization of flow conditions. They cannot represent the dynamics of the panel for other realizations of flow conditions. One can utilize response surface methodology to represent variation of the coefficients of the model terms with respect to variations in flow conditions. The accuracy of the models generated using such approach will depend on the accuracy and interpolation or extrapolation capability of the fitted response surfaces.

Acknowledgments

This research was supported by the Dayton Area Graduate Studies Institute contract ML-OSU-00-09 and AFRL/VA contract F33615-98-D-3210, monitored by Christopher Pettit. The authors are grateful to Sean Mortara and Philip Beran for their assistance in completing this effort.

References

[1]Juang, J.-N., *Applied System Identification*, Prentice–Hall, Englewood Cliffs, NJ, 1994, pp. 121–255.

[2]Billings, S., "Identification of Nonlinear Systems: A Survey," *IEEE Proceedings*, Vol. 11, Part D, No. 6, 1980, pp. 272–285.

[3]Mook, D., and Junkins, J., "Minimum Model Error Estimation for Poorly Modeled Dynamic Systems," *Journal of Guidance, Control, and Dynamics*, Vol. 11, No. 3, 1988, pp. 256–261.

[4]Stry, G., "MME Nonlinear Dynamic System Identification," Ph.D. Dissertation, School of Engineering and Applied Science, Univ. of New York, Buffalo, NY, Aug. 1991.

[5]Crassidis, J. L., and Markley, F. L., "Minimum Model Error Approach for Attitude Estimation," *Journal of Guidance, Control, and Dynamics*, Vol. 20, No. 6, 1997, pp. 1241–1247.

[6]Baldelli, D. H., Chen, P. C., Liu, D. D., Lind, R., and Brenner, M., "Nonlinear Aeroelastic Modeling by Block-Oriented Identification," AIAA Paper 2004-1938, April 2004.

[7]Marzocca, P., Lazzaro, R., and Librescu, L., "Flutter/Aeroelastic Response of Panels via a Combined Galerkin-Volterra Series Approach," AIAA Paper 2004-1855, April 2004.

[8]Prazenica, R. J., Reisentel, P. H., Kurdila, A. J., and Brenner, M. J., "Volterra Kernel Identification and Extrapolation for the F/A-18 Active Aeroelastic Wing," AIAA Paper 2004-1939, April 2004.

[9]Geering, H., "Continuous Time Optimal Control Theory of Cost Functionals Including Discrete State Penalty Terms," *IEEE Transactions A. C.*, Vol. AC-21, No. 6, 1976, pp. 979–983.

[10]Mook, D. J., and Lew, J.-S., "Multiple Shooting Algorithms for Jump-Discontinuous Problems in Optimal Control and Estimation," *IEEE Transactions, A. C.*, Vol. 36, No. 8, 1991, pp. 979–983.

[11]Mook, D., and Stry, G., "Correlation Techniques in Robust Nonlinear System Realization/Identification," 32nd AIAA/ASME/ASCE/AHS/ASC Structures, Structural Dynamics, and Materials Conference, April 1991, Technical Papers. Pt. 4 (A91-31826 12-39), pp. 2786–2795.

[12]Dowell, E., "Nonlinear Oscillations of a Fluttering Plate," *AIAA Journal*, Vol. 4, No. 7, 1966, pp. 1267–1275.

[13]Mortara, S., "Advanced Computational Aeroelastic Methods," M.S. Thesis, Dept. of Mechanical and Materials Engineering, Wright State Univ., Dayton, OH, Aug. 2002.

[14]Holmes, P., Lumley, J., and Berkooz, G., *Turbulence, Coherent Structures, Dynamical Systems and Symmetry*, Cambridge Univ. Press, New York, 1996, pp. 86–128.

[15]Epurenau, B. I., and Dowell, E. H., "Compact Methodology of Computing Limit-Cycle Oscillations in Aeroelasticity," *Journal of Aircraft*, Vol. 40, No. 5, 2003, pp. 955–963.

[16]*Using MATLAB*, The MathWorks, Inc., Natick, MA, July 2002.

[17]Gopinathan, A., "Robust Nonlinear System Identification Using Correlation Techniques," M.S. Thesis, Dept. of Mechanical and Materials Engineering, Wright State Univ., Dayton, OH, Dec. 1999.